J. Fluid Mech. (1977), *vol.* 79, *part* 4, *pp.* 785–799
Printed in Great Britain

Asymptotic similarity of turbulence structures in smooth- and rough-walled pipes

By A. E. PERRY

Department of Mechanical Engineering, University of Melbourne, Parkville, Victoria 3052, Australia

AND C. J. ABELL

Department of Mechanical Engineering, University of Adelaide, South Australia

(Received 29 August 1975 and in revised form 4 September 1976)

Work recently reported by the authors (Perry & Abell 1975) on smooth-walled pipe flow showed support for the Townsend (1976) structural similarity principle as regards viscosity not being directly relevant in controlling the mean relative motions and the energy-containing turbulent motions. The work also supported a universal spectral behaviour in the wall region of the flow. In many hypotheses for rough-walled pipe flow, surface roughness, like viscosity, enters the problem only via external boundary conditions. Data obtained in a rough pipe are reported here and on first appearance the results seem to contradict the Townsend hypothesis and to threaten the very foundation upon which many similarity laws for rough-walled flows are based. However, on closer examination of the spectrum scaling of smooth-walled pipe flow the low and high wavenumber energy not necessarily associated with the universal similarity range can be accounted for. The broad-band longitudinal turbulence results for a rough-walled pipe can then be predicted from the smooth-wall scaling. The conclusion is that, despite the apparent anomalies, the turbulence structure in a rough pipe appears to follow the same scaling laws as for a smooth pipe, given a sufficient length of flow development in both cases. The deduced functional forms are consistent with Townsend's (1976) attached-eddy hypothesis.

1. Introduction

The authors interpret the Townsend (1976) Reynolds number similarity hypothesis, when applied to fully developed pipe flow, to mean the following. All mean *relative* motions and energy-containing components of the turbulent motions are independent of viscosity and surface roughness except in so far as these variables may affect the boundary conditions on the flow. This will be referred to here as simply the 'Townsend hypothesis' and is presumed to be valid across the entire pipe cross-section except for thin viscous and roughness zones very close to the pipe walls.

The velocity defect law for the mean flow follows from this hypothesis, and viscosity or surface roughness influences only the value of the shear velocity

u_τ and the velocity of 'slip' at the boundary for a given velocity U_1 at the pipe axis and given pipe radius R. Postulates about an 'inner law' and a region of overlap with the defect law lead to a logarithmic distribution of mean velocity over some "possibly small but finite region" (Millikan 1938). The mean flow data have been very successfully correlated in this way, but attempts to correlate turbulence quantities such as $\overline{u^2}/u_\tau^2$ (where u is the streamwise velocity fluctuation and the overbar represents a time average) using analogous techniques have been far from satisfactory. Much of the reason for this has been poor calibration techniques for the instruments used to measure the velocity fluctuations. Perry & Abell (1975) succeeded in obtaining what appeared to be a consistent set of data by using very careful dynamic calibration methods (Perry & Morrison 1971). By postulating a region of overlap between an inner law and an outer law, a region where $\overline{u^2}/u_\tau^2 = H$ (a universal constant) can be deduced. Their measurements apparently confirmed this deduction for smooth pipes for the Reynolds number range $Re = 80 \times 10^3$ to 260×10^3 (based on pipe diameter d and centre-line velocity U_1) and they tentatively set the region of validity as $y_+ > 100$ and $y/R < 0{\cdot}1$. (Here y is the distance normal to the wall and $y_+ = yu_\tau/\nu$, where ν is the kinematic viscosity.) This corresponds closely to the region of validity of the logarithmic law for the mean flow. Hence it would appear that the turbulence quantities are as well behaved as the mean flow quantities, as most workers either expected or hoped. However, as will be seen later, the whole problem of the scaling of turbulence intensities is far more complex and it seems unlikely that a universal value for H is applicable.

Difficulties start to appear when one considers the turbulence spectra. Perry & Abell proposed that in the region of constant $\overline{u^2}/u_\tau^2$ (referred to here as the wall region) a universal wall similarity is valid for the energy-containing motions, i.e.

$$\Phi(k)/yu_\tau^2 = f_1(ky), \tag{1}$$

where k is the longitudinal wavenumber and the energy spectrum function $\Phi(k)$ is normalized to give

$$\int_0^\infty \Phi(k)\,dk = \overline{u^2}.$$

Although this proposal showed a considerable improvement in data correlation over past proposals, the scatter in the results cannot be explained by experimental error. The low wavenumber range shows systematic departures and these motions contain appreciable energy. These departures have been noted by many authors and are often referred to as the 'inactive' motions. The authors prefer to call them the 'non-universal' motions, as distinct from those satisfying (1), the 'universal' motions. It is hoped that the formulation for the latter can be transferred to other flows (boundary layers, rectangular ducts, etc.) while the former motions are particular to a given large-scale external geometry.

The best way of explaining one cause of the scatter in the spectra is that all results were obtained using an electronic filter whose sensing element was fixed in laboratory co-ordinates. This gives frequency signals which depend on the velocity of convection of the turbulence structure past the transducer. The basis of the Townsend hypothesis is that *absolute* velocities are not involved, only

relative motions. A stationary filter generates contaminated spectral estimates and the spectra should really be expressed in terms of quantities which are invariant with the velocity of the observer. A spectral form which contains such quantities can be derived from a function suggested by Ffowcs Williams (e.g. see Wills 1964):

$$W(k,c) = \frac{1}{(2\pi)^2}\iint_{-\infty}^{\infty} \overline{u^2}R(\delta,\tau)\exp\{ik(\delta - c\tau)\}\,d\delta\,d\tau,$$

where $R(\delta,\tau)$ is the two-point space–time correlation coefficient, δ is the streamwise spacing of the sensing elements and τ is a time shift.

The function W is expressed in terms of the wavenumber k and phase velocity c. Now it can be shown that if $W_0(k,c)$ is the spectrum function measured by an observer in laboratory co-ordinates, then the spectrum function W_V measured by an observer moving with velocity V is given by

$$W_V(k,c) = W_0(k, c-V).$$

This means that $W(k,c)$ contours translate without distortion on the k,c plane for a change in velocity of the observer and hence it is possible to express W_V in terms of *relative* phase velocities which are independent of the observer. By convention let $V = U$ in what follows.

Expressed in non-dimensional terms, the universal wall similarity hypothesis then becomes

$$\frac{W}{yu_\tau} = f_2\left(ky, \frac{c-U}{u_\tau}\right). \tag{2}$$

One would expect the small-scale motions to be convected at the local mean velocity U with a small spread in phase velocity whereas motions of very large scale would be convected at a velocity closer to U_1. These large-scale motions cause the slow 'sloshing' around of the viscous sublayer (at frequencies scaling on outer-flow variables) as the large-scale motions travel faster than the fine-scale motions closer to the boundary. Hence at low non-dimensional wavenumber ky, one would expect a spread in phase velocity of the order of $(U-U_1)/u_\tau$. Now, from the logarithmic defect law

$$(U-U_1)/u_\tau = \kappa^{-1}\ln y/R - C, \tag{3}$$

where κ and C are universal constants. Thus in view of (3), (2) must be modified to include y/R as a parameter for the low wavenumber range, giving

$$\frac{W}{yu_\tau} = f_3\left(ky, \frac{c-U}{u_\tau}, y/R\right). \tag{4}$$

Figure 1 shows conjectural contours of W/yu_τ for three different relative velocities of the observer for a given y/R. The relative velocity can be varied in a number of ways if the observer is fixed to laboratory co-ordinates: one way is to change the Reynolds number of the flow and another is to retard the flow locally by surface roughness, the retardation being the roughness function $\Delta u/u_\tau$ (see Hama 1954; Clauser 1954).

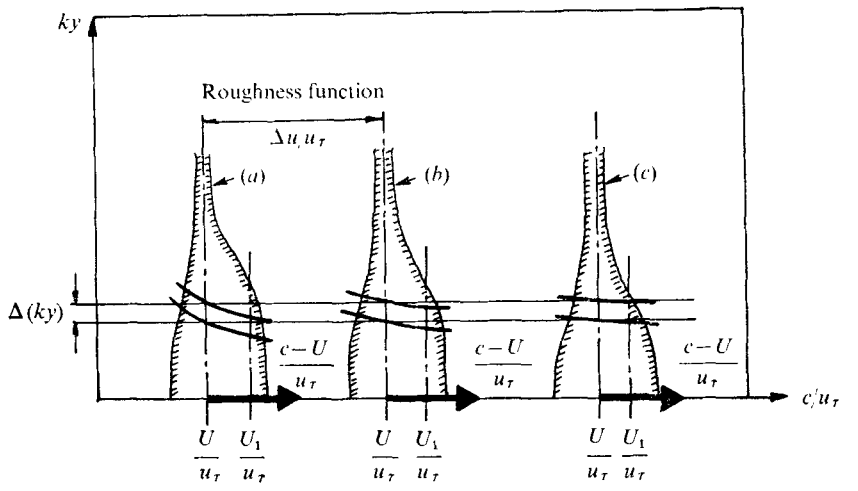

FIGURE 1. Conjectured contours of the spectrum function W/yu_τ. (*a*) Rough-wall case. (*b*) Smooth wall; same Reynolds number. (*c*) Smooth wall; high Reynolds number. The shaded areas represent energy-containing regions.

The function $\Phi(k)/yu_\tau^2$ is obtained by integrating $W(k,c)/yu_\tau$ along horizontal strips $\Delta(ky)$ wide. However, a stationary observer with a frequency-band filter will be integrating along hyperbolic strips of width $\Delta(\omega y/u_\tau)$.

For a smooth-walled pipe, as $Re\to\infty$, Ru_τ/ν $(=R_+)\to\infty$ and, since

$$U_1/u_\tau = \kappa^{-1}\ln R_+ + D$$

(where D is a universal constant), $U_1/u_\tau\to\infty$. Hence $(U_1-c)/U_1$ (the fractional spread in phase velocity) diminishes, and so for large U_1/u_τ one can use the Taylor transformation

$$k = \omega/U \tag{5}$$

since then the hyperbolic strips contain the same energy as the horizontal strips, and U will be approximately U_1. If $P(\omega)$ is the power spectrum measured by a stationary filter, then $\Phi(k)$ tends towards $UP(\omega)$ with increasing U_1/u_τ and

$$\int_0^\infty P(\omega)\,d\omega = \overline{u^2}. \tag{6}$$

However, at low U_1/u_τ and low ky, the inferred spectrum $\Phi(k)$ obtained from $P(\omega)$ using (5) could be distorted because the hyperbolic strips cut the energy-containing contours in a different manner to the horizontal strips. Also the contours might peak at a phase velocity c substantially different from U. From the figure one would expect estimates of $\Phi(k)$ for rough-walled pipe flow obtained by measuring $P(\omega)$ to be highly distorted. What is really needed is a direct mapping of $W(k,c)/yu_\tau$ obtained from measurements of $R(\delta,\tau)$, a tedious process requiring two hot wires one behind the other, with the inevitable flow interference. Laser-Doppler methods look hopeful if the measuring volume could be made sufficiently small and if the problems of signal drop-out and frequency broadening could be resolved. Until these difficulties are overcome one must be content with the 'electronic filter' function $P(\omega)$.

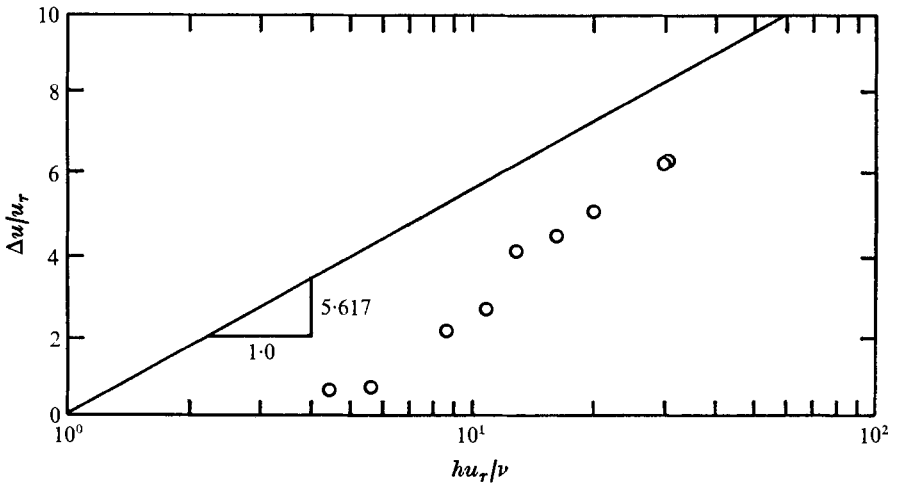

FIGURE 2. Measured variation of the roughness function $\Delta u/u_\tau$ in the rough-walled pipe. h is the roughness height.

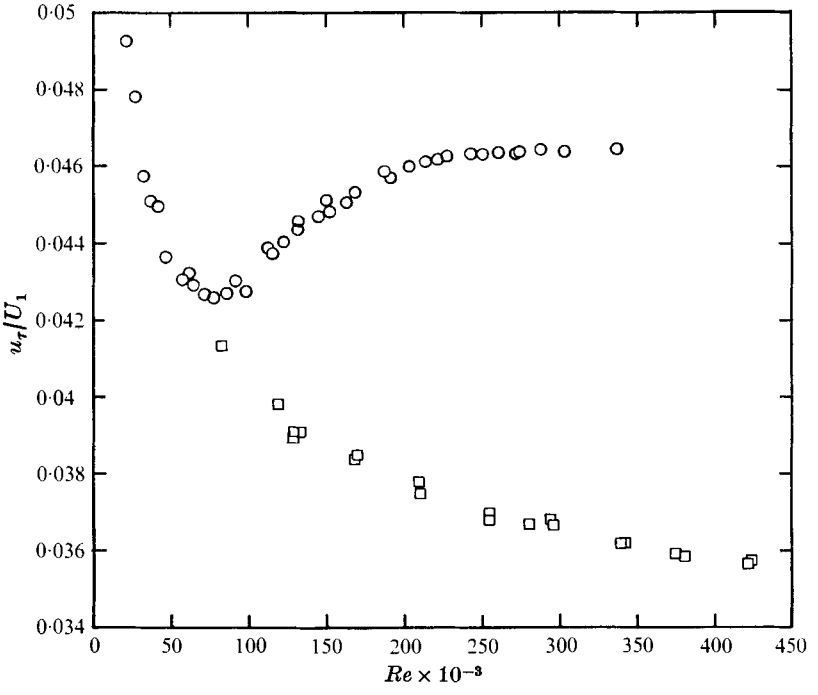

FIGURE 3. Measured variation of shear velocity with Reynolds number for both smooth- and rough-walled pipes. ○, rough wall; □, smooth wall.

Recent experiments carried out by the authors with a rough pipe gave broad-band results which differed appreciably from the results for smooth-walled pipe flow. Since these are broad-band data, the velocity of the observer cannot explain the anomaly. The authors consider this result significant and disturbing in that it suggests a dependence of broad-band turbulence structure on the

physical details of the inner boundary conditions. It is shown here that a likely explanation is that the smooth-walled pipe flow had not reached its asymptotic state. From a careful examination of the measured spectra, the correct asymptotic state can be predicted, which shows the two sets of data to be compatible.

2. The rough-walled pipe

For the rough-wall measurements the inlet contraction used for the smooth-walled pipe (see Perry & Abell 1975) was attached to a thick-walled steel tube of internal diameter 0·102 m. To enable the roughness to be fitted to the internal surface, the pipe was cut into six equal lengths and, after annealing to reduce residual stresses, each length was slit longitudinally and accurately shimmed each side. By turning the outside diameter of both ends of each length concentric to the bore, the sections could be fitted together with minimal irregularities at the joins. The roughness used was nylon mesh of hexagonal weave (cell size 2·5 mm) and nominal height 0·25 mm.

The variation of the roughness function $\Delta u/u_\tau$, obtained from the mean flow profiles, is shown in figure 2, and figure 3 shows the Reynolds number variation of u_τ/U_1, obtained from static-pressure measurements. The figures suggest that the rough-walled pipe flow is in the fully rough regime for $Re > 280 \times 10^3$.

3. The energy chain in pipe flow

The hypothesis of universal wall structure

In the region of universal wall structure

$$\Phi(k)/yu_\tau^2 = f_1(ky), \tag{7}$$

where $\Phi(k)$ is the energy per unit 'inferred' wavenumber, obtained using (5). If this were valid over the entire wavenumber range of the spectrum then

$$\int_0^\infty f_1(ky)\, d(ky) = \overline{u^2}/u_\tau^2. \tag{8}$$

However, (7) must break down at very low wavenumbers where the large-scale geometry of the apparatus has an influence, and at the wavenumbers sufficiently high for viscous dissipation to have an effect.

Low wavenumber range

In the low wavenumber range, (7) must be reformulated to include the pipe radius and, at extremely low wavenumbers, perhaps the length of the pipe L. Ignoring the effect of L for the time being we have

$$\Phi(k)/yu_\tau^2 = f_4(y/R, ky). \tag{9}$$

Of course $\Phi(k)$ cannot really be obtained from $P(\omega)$ by the simple Taylor transformation (5) since the structure has a phase velocity quite different from the local mean velocity U. The phase velocity would be nearer U_1, possibly with a

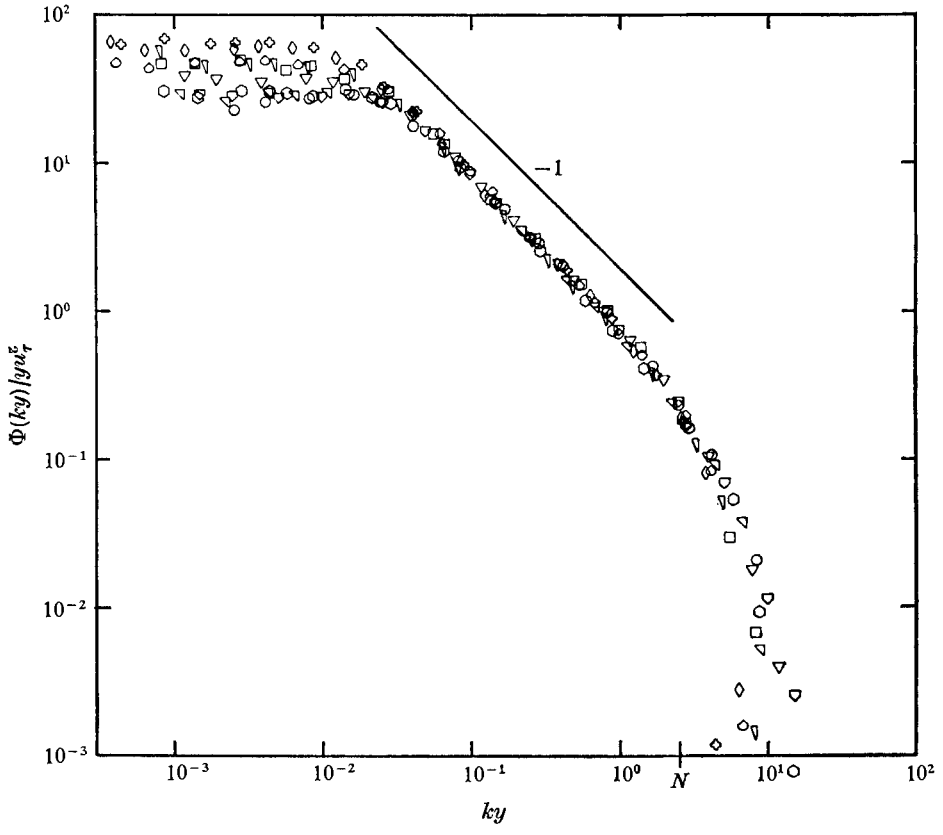

FIGURE 4. Smooth-wall longitudinal turbulence spectra for the wall-distance range $y_+ > 100$ and $y/R < 0{\cdot}1$. Reynolds number range = 80×10^3 to 260×10^3, symbols as for figure 11 of Perry & Abell (1975).

wide spread for a given ky, and it is only at unattainably high Reynolds numbers in a smooth pipe that the Taylor hypothesis will become valid at small y/R for these large-scale motions. Let it be assumed, however, that the actual form of $\Phi(k)$ is known.

An overlap of (7) and (9) leads to a particular form for the spectrum function:

$$\Phi(k)/u_\tau^2 y = A/ky \tag{10a}$$

or

$$\Phi(k)/u_\tau^2 R = A/kR. \tag{10b}$$

This form was suggested by Abell (1974) and was deduced on the basis of the requirement that $\Phi(k)$ as given by (9) must be independent of the wall distance y. Equation (9) then becomes completely consistent with (10) in the region of overlap. Experiment certainly indicates extensive regions where (10) is valid, indicating a substantial overlap region. (See figure 4.) A noteworthy feature of (10) is that it is valid independent of the velocity of the observer. The data points simply shift along the line of slope -1 shown in figure 4, irrespective of whether or not the inferred wavenumber is correct.

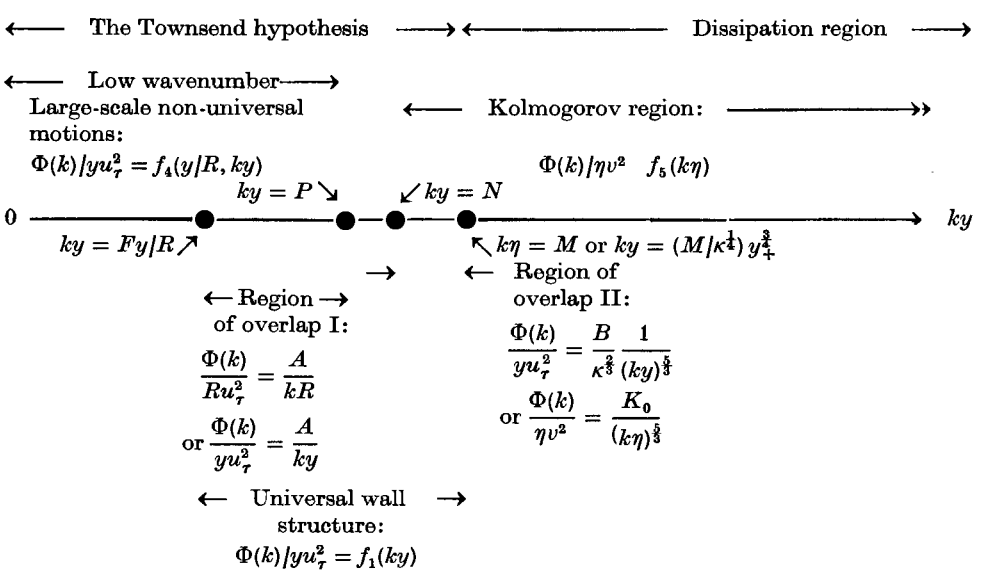

TABLE 1. The energy chain in a pipe.

High wavenumber range

It could be speculated that in pipe flow the dissipation and energy-containing ranges strongly overlap, i.e. the eddies are produced and dissipated without substantial energy transfer. The authors proceed with the more conventional view that viscosity plays no part in the range of universal wall structure, but that there exists a Kolmogorov region, in which

$$\Phi(k)/\eta v^2 = f_5(k\eta), \tag{11}$$

where the function f_5 is universal and η and v are the Kolmogorov length and velocity scales, given by

$$\eta = (\nu^3/\epsilon)^{\frac{1}{4}}, \quad v = (\nu\epsilon)^{\frac{1}{4}}, \tag{12}$$

where ϵ is the dissipation.

For purposes of calculation, a good assumption is Townsend's (1961) proposal that in the fully turbulent part of the wall region production of energy is in balance with dissipation. Here the production p is

$$p = -\overline{uv}\,\partial U/\partial y \tag{13}$$

and for sufficiently small y/R

$$p = \epsilon = u_\tau^3/\kappa y. \tag{14}$$

This gives

$$v = (\nu u_\tau^3/\kappa y)^{\frac{1}{4}}, \quad \eta = (\nu^3 \kappa y/u_\tau^3)^{\frac{1}{4}}. \tag{15}$$

The dissipation range begins at a universal value of $k\eta = M$, corresponding to

$$ky = (M/\kappa^{\frac{1}{4}})\, y_+^{\frac{3}{4}}, \tag{16}$$

where $y_+ = yu_\tau/\nu$.

A region of overlap between the dissipation region and what is referred to here as the universal wall region, where (7) holds, implies isotropic properties for

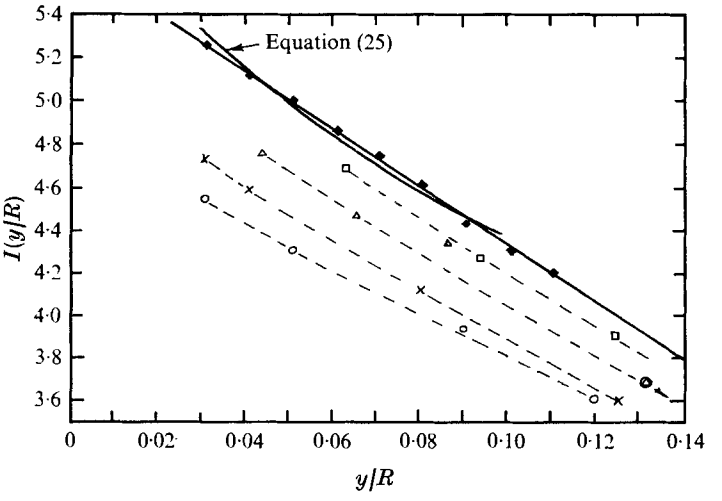

FIGURE 5. The integral $I_1(y/R)$ obtained from (22) and the smooth-pipe data with $B = 1{\cdot}37$, $M = 0{\cdot}08$, $N = 2{\cdot}154$ and $\kappa = 0{\cdot}41$. ◆, asymptotic curve, I_1 (as a function of y/R only) obtained by extrapolation of curves in figure 6.

	□	△	×	○
Re	80×10^3	120×10^3	180×10^3	260×10^3
u_τ/U_1	0·0415	0·0390	0·0378	0·0368

these small-scale motions, and the region of overlap is commonly termed the 'inertial subrange'. In this inertial subrange (11) is valid but ν is not involved explicitly. This leads to the well-known result that

$$\Phi(k)/\eta v^2 = K_0/(k\eta)^{\frac{5}{3}}, \tag{17}$$

where K_0 is the Kolmogorov constant. By the use of (15), (17) becomes

$$\frac{\Phi(k)}{u_\tau^2 y} = \frac{K_0}{\kappa^{\frac{2}{3}}} \frac{1}{(ky)^{\frac{5}{3}}}, \tag{18}$$

which is recognizable as a particular form of (7). Thus the spectrum and the various wavenumber regions can be summarized as in table 1.

4. Estimation of the spectral-energy contribution from smooth-pipe data

Figure 4 shows the measured spectra for the smooth-walled pipe. Integrations with respect to ky are performed over the following regions to obtain broad-band contributions:

$$0 < ky \leqslant N, \quad \Phi(k)/yu_\tau^2 = f_4(y/R, ky), \tag{19}$$

$$N < ky \leqslant M\kappa^{-\frac{1}{4}} y_+^{\frac{3}{4}}, \quad \Phi(k)/yu_\tau^2 = B(ky)^{-\frac{5}{3}}, \tag{20}$$

where $B = K_0 \kappa^{-\frac{2}{3}}$. Hence

$$\frac{\overline{u^2}}{u_\tau^2} = \int_0^N f_4(y/R, ky)\, d(ky) + \int_N^{M\kappa^{-\frac{1}{4}} y_+^{\frac{1}{4}}} B(ky)^{-\frac{5}{3}}\, d(ky)$$

$$= I_1(y/R) + I_2(y_+). \tag{21}$$

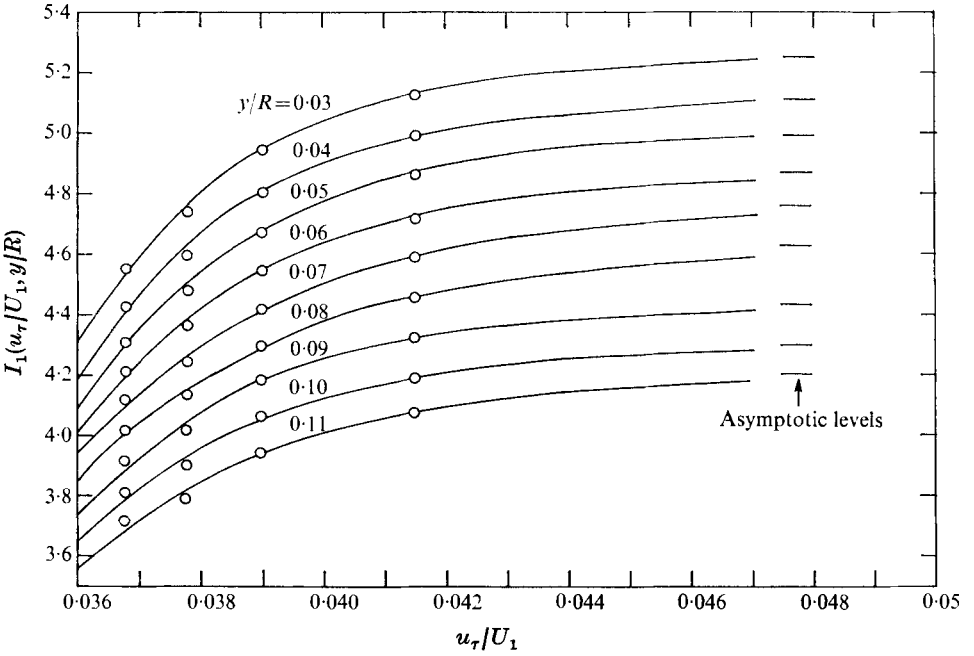

FIGURE 6. Cross-plot of the results shown in figure 5. (The data points are experimental and the full curves are from the fit to the data.)

In (21) the first term I_1 gives the total amount of energy outside the Kolmogorov range. The energy contribution of the dissipation range of wavenumbers, typically $O(\frac{1}{10}I_2)$, is neglected, but account is taken of the growth of the range of universal wall similarity with y_+, and all large-scale motions are included in the integral $I_1(y/R)$.

From (21),

$$I_1(y/R) = \frac{\overline{u^2}}{u_\tau^2} - \frac{3}{2}\frac{B}{N^{\frac{2}{3}}} + \frac{3}{2}\frac{B\kappa^{\frac{1}{6}}}{M^{\frac{2}{3}}y_+^{\frac{1}{2}}}. \tag{22}$$

Using the measured values of $\overline{u^2}/u_\tau^2$ and estimates of B, N and M, obtained from the data of figure 4, with $\kappa = 0{\cdot}41$, $I_1(y/R)$ was evaluated using (22) and is shown in figure 5.

Estimation of I_1 from (22) does not require any assumptions about the form of the low wavenumber range and avoids the direct integration of that part of the spectrum most likely to be contaminated by invalid use of the Taylor transformation. The resulting $I_1(y/R)$ shows a significant and apparently systematic trend with Reynolds number. This is impossible for a fully developed flow since the large-scale motion must be independent of viscosity. An alternative parameter to attach to the curves is u_τ/U_1, but, again, this contradicts the Townsend hypothesis since absolute velocities like U_1 should not enter if the results are uncontaminated.

Contamination by u_τ/U_1 may arise from four possible physical sources.

(i) Additional turbulence produced via the screens and the contraction at the pipe entrance. However this would show the opposite Reynolds number trend.

(ii) Fixed-frequency high-pass filtering of the anemometer signals, causing differing proportions of broad-band energy to be cut off. Again the trend is the wrong way.

(iii) Area-normalization of measured spectra to $\overline{u^2}/u_\tau^2$. Since at low wavenumbers the inferred $\Phi(k)$ is in error because of the large difference in phase velocities, estimates of the constant B could be in error. However, the trend with u_τ/U_1 cannot be removed by changing the value of B.

(iv) Lack of sufficient flow-development length. This seems the most likely, and support for this was obtained by cross-plotting the data as shown in figure 6.

Here it can be seen that I_1 becomes independent of u_τ/U_1 for u_τ/U_1 sufficiently large. The asymptotic form of $I_1(y/R)$ is shown in figure 5 as the solid line. For a smooth-walled pipe flow, the asymptote is reached by decreasing the Reynolds number. If viscosity were causing the trends directly, one would expect to reach asymptotic behaviour by increasing the Reynolds number. Thus viscosity must be entering via its influence on some large-scale boundary condition. Further, the wavenumbers at which these departures occur have values approaching the order of the reciprocal of the length of the pipe. These points support the view that insufficient development length is the cause, and this is consistent with the u_τ/U_1 trends.

For the purposes of order-of-magnitude calculations, the boundary layers in the entrance length of the pipe are considered approximately self-preserving, with u_τ/U_1 approximately constant over most of the development length. As the boundary layers grow, they finally meet and, after a settling length, fully developed flow is achieved. If the development length is approximated as proportional to the length required for the layers to meet, then

$$l/d \propto (u_\tau/U_1)^{-2} \tag{23}$$

(from approximate two-dimensional boundary-layer theory with $d\theta/dx = (u_\tau/U_1)^2$, where θ is the momentum thickness).† The higher u_τ/U_1, the more rapid will be the boundary-layer growth. For rough pipes u_τ/U_1 is substantially higher for the same flow Reynolds number, giving a very rapid growth rate.

5. Prediction of results for rough-walled pipes

The large-scale geometry of the rough-pipe apparatus was identical in all respects to that used in the smooth-pipe experiments. The measuring station was located at the same number of pipe diameters from the entrance in both cases (84·7).

By using the experimental mapping of $I_1(y/R,\ u_\tau/U_1)$ obtained from the smooth-wall experiment (shown in figure 5) with some extrapolation, the broad-band $\overline{u^2}/u_\tau^2$ distributions can be predicted for the rough-pipe flows given u_τ/U_1 and either R_+ or Re. The correlation between the data and the predictions is shown in figure 7. No new constants whatsoever have been introduced for the

† A simple analysis based on (23) with $u_\tau/U_1 = 0{\cdot}04$ (typical for smooth-pipe flows) suggests that l/d should be *at least* 150 for the flow to approach fully developed conditions for this particular case.

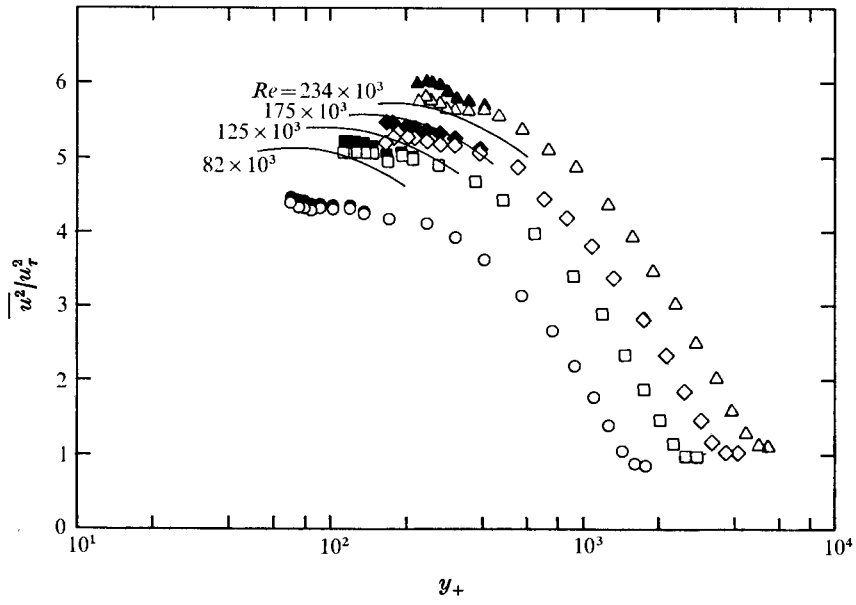

FIGURE 7. Comparison of rough-wall broad-band turbulence data with predictions based on the smooth-wall results. The full curves were obtained from (21) with $I_1(y/R, u_\tau/U_1)$ taken from figure 6.

	○	□	◇	△
Re	82×10^3	125×10^3	175×10^3	234×10^3
u_τ/U_1	0·0427	0·04415	0·0455	0·0463

Closed symbols represent measurements corrected for the spatial averaging effect of hot wires (using the method of Wyngaard 1968); open symbols show uncorrected data.

rough-pipe calculations. Thus the assertion that rough-walled pipe flow obeys the same structural similarity laws as smooth-walled pipe flow receives encouraging support. The departures from the data could well be caused by the extrapolation procedure. The trends and the order of magnitude of the change from smooth- to rough-pipe data are predicted reasonably well.

6. Asymptotic broad-band profiles

For $xd^{-1}(u_\tau/U_1)^2$ large, where x is the streamwise distance from the pipe entrance, it should be possible to predict the complete family of $\overline{u^2}/u_\tau^2$ profiles.

The functional form of $I_1(y/R)$ for fully developed flow can now be deduced. For very low wavenumbers, (10*b*) can be generalized to read

$$\Phi(k)/Ru_\tau^2 = f_5(kR). \tag{24}$$

This is consistent with the physical argument that the scale of very large motions will be limited by the size of the pipe and their contributions to $\overline{u^2}/u_\tau^2$ will be fairly insensitive to y for low y/R ($< 0{\cdot}1$). This equation will gradually merge into (10*b*) for increasing kR. Let F be the universal value of kR at which this merging begins.

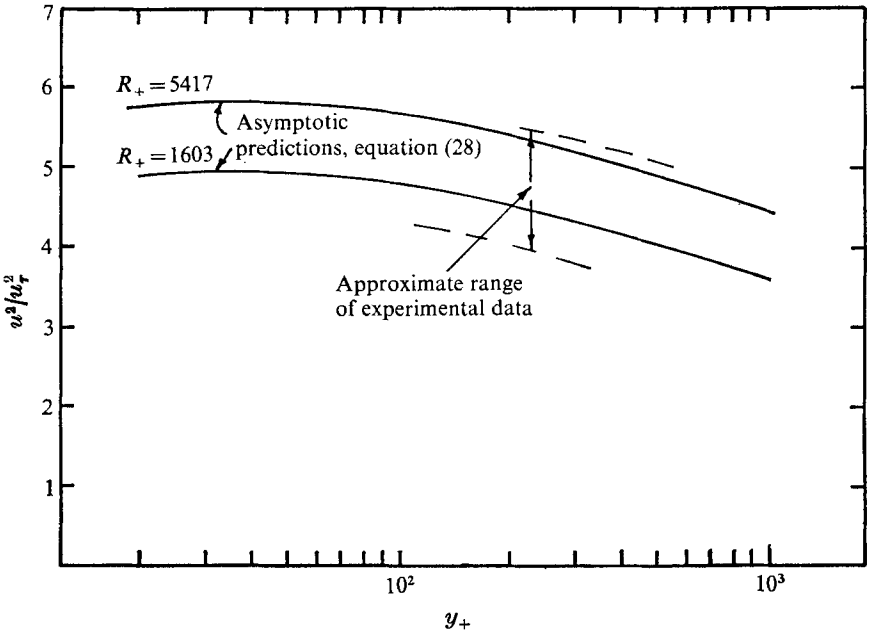

FIGURE 8. Equation (28) for full range of R_+ used.

Experimental data also show that (10*a*) is valid almost up to $ky = N$. Hence, with the aid of (10*a*), the integral

$$I_1\left(\frac{y}{R}\right) = \int_0^N \frac{\Phi(k)}{yu_\tau^2}\, d(ky)$$

may be written as

$$I_1\left(\frac{y}{R}\right) = \int_0^F \frac{\Phi(k)}{Ru_\tau^2}\, d(kR) + \int_{F.y/R}^N \frac{\Phi(k)}{yu_\tau^2}\, d(ky).$$

The first integral is a characteristic constant for circular pipes and the second integral will be logarithmic. After regrouping various constants this gives

$$I_1(y/R) = Q - A\ln(y/R). \tag{25}$$

From the spectrum function $A \simeq 0{\cdot}8$, and by curve fitting to the extrapolated results shown in figure 5, $Q \simeq 2{\cdot}3$. Also shown in the figure is a linearized approximation $I_1 = 5{\cdot}66 - 13{\cdot}3(y/R)$, which is valid provided that $0{\cdot}03 < y/R \leqslant 0{\cdot}1$.

From (21)

$$I_2 = T - cy_+^{-\frac{1}{2}}, \tag{26}$$

where $T = 1{\cdot}23$ and $c = 9{\cdot}54$. Hence from (25) and (26)

$$\overline{u^2}/u_\tau^2 = S - A\ln(y/R) - cy_+^{-\frac{1}{2}}, \tag{27}$$

where $S \simeq 3{\cdot}53$. Equation (27) can also be written as

$$\overline{u^2}/u_\tau^2 = S - A\ln y_+ + A\ln R_+ - cy_+^{-\frac{1}{2}}. \tag{28}$$

Equation (28) is plotted in figure 8 for the full range of R_+ considered in this paper, covering all the smooth- and rough-wall results. Also shown is the corresponding

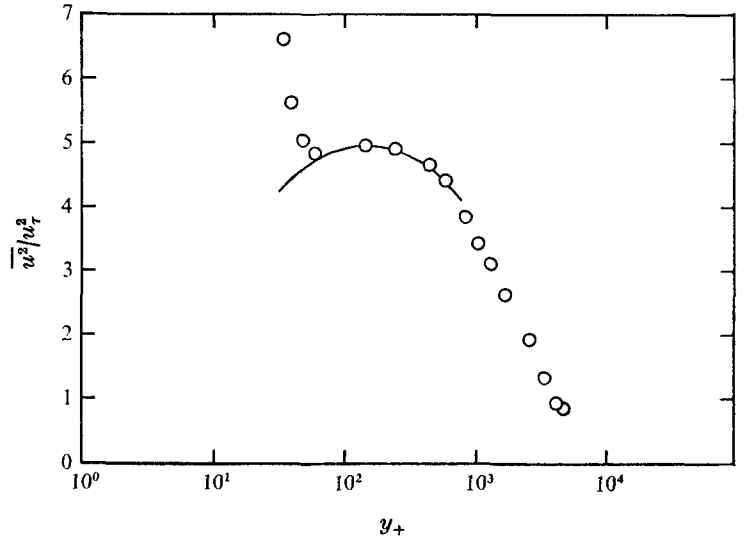

FIGURE 9. Non-asymptotic case. Smooth-walled pipe, $Re = 2{\cdot}6 \times 10^5$, $u_\tau/U_1 = 0{\cdot}0368$, $x/d = 84{\cdot}7$. The full curve was obtained from (21) and figure 5.

spread of experimental data. Experimental results and asymptotic predictions appear to agree for the highest (rough wall) R_+ values.

The presence of the logarithmic singularity in (27) is consistent with the deductions of Townsend (1976), who arrived at a similar result via a quite different line of reasoning using his attached-eddy hypothesis. In laboratory turbulence, the effect of this singularity on a $\overline{u^2}/u_\tau^2$ *vs.* y/R plot would be weak since low values of y/R cannot be achieved outside the viscous or roughness zones because of an insufficiently large R_+. However, in atmospheric turbulence, the effect could be strong.

7. Non-asymptotic predictions

For flow situations without a sufficient development length the function $I_1(y/R, u_\tau/U_1)$ must be used. For the particular situation $x/d = 84{\cdot}7$ one case of interest is $Re = 2{\cdot}6 \times 10^5$. The asymptotic case given by (28) had not been reached and the values of I_1 given in figure 5 were used. The resulting profile 'kicks up' slightly as shown in figure 9. Such behaviour is typical of flows with an insufficient length of flow development. I. A. Hunt (Department of Mechanical Engineering, University of Melbourne, private communication) has recorded similar profiles in flows in rectangular ducts of high aspect ratio.

8. Conclusions

From a study of smooth-walled pipe flow, longitudinal turbulence energy spectra and the various regions and governing variables have been proposed. Careful examination of the scaling of these spectra suggests that the data of

Perry & Abell (1975) had not reached an asymptotic state. By extrapolation of the spectral laws derived from the data, the asymptotic state can be predicted and has been shown to be consistent with results for rough-walled pipe flow, which approach asymptotic conditions more rapidly than did the smooth-pipe results.

Provided the length of flow development is sufficiently large compared with $d(u_\tau/U_1)^{-2}$, the broad-band longitudinal turbulence profile in the wall region can be expressed as [equation (28)]

$$\overline{u^2}/u_\tau^2 = S - A\ln y_+ + A\ln R_+ - cy_+^{-\frac{1}{2}}, \tag{29}$$

where $S = 3{\cdot}53$, $A = 0{\cdot}8$ and $c = 9{\cdot}54$. A and c are universal constants and hopefully could be used in other flows such as rectangular ducts or boundary layers. However, the constant S is particular to circular pipe flow. Contributions to this constant are made by the universal motions and by the non-universal motions. The ratio of these contributions will not be known until the spectral function $W(k, c)$ has been mapped out.

By assuming a region of overlap in the spectrum between the low wavenumber non-universal motions and the high wavenumber universal motions a logarithmic distribution in $\overline{u^2}/u_\tau^2$ can be deduced. This is consistent with Townsend's attached-eddy hypothesis.

Until further work is carried out, the authors tentatively set the region of validity for (28) as $y^+ \geqslant 100$ and $y/R < 0{\cdot}1$, which is also the region of validity of the logarithmic law for the mean flow.

The authors wish to thank Dr A. A. Townsend for many stimulating discussions and for pointing out the consistency of the authors' spectral formulations with his attached-eddy hypothesis. The authors also wish to acknowledge the financial support of the Australian Research Grants Committee and the Australian Institute of Nuclear Science and Engineering.

REFERENCES

ABELL, C. J. 1974 Ph.D. thesis, University of Melbourne.

CLAUSER, F. H. 1954 *J. Aero. Sci.* **21**, 91.

HAMA, F. R. 1954 *Trans. Soc. Naval Arch. Mar. Engrs*, **62**, 333.

MILLIKAN, C. D. 1938 *Proc. 5th Int. Cong. Appl. Mech.*, pp. 386–392.

PERRY, A. E. & ABELL, C. J. 1975 *J. Fluid Mech.* **67**, 257–271.

PERRY, A. E. & MORRISON, G. L. 1971 *J. Fluid Mech.* **47**, 765–777.

TOWNSEND, A. A. 1961 *J. Fluid Mech.* **11**, 97–120.

TOWNSEND, A. A. 1976 *The Structure of Turbulent Shear Flow*, 2nd edn, pp. 150–158. Cambridge University Press.

WILLS, J. A. B. 1964 *J. Fluid Mech.* **20**, 417.

WYNGAARD, J. C. 1968 *J. Phys.* E **1**, 1105.